Journal of Flow Chemistry (2021) 11:345–355
https://doi.org/10.1007/s41981-021-00170-5

FULL PAPER

Study of propane/air catalytic combustion in heat recirculating U-bend and spiral microcombustors

Aswathy K. Raghu [1] · Niket S. Kaisare [1]

Received: 19 December 2020 / Accepted: 27 April 2021 / Published online: 17 May 2021

Abstract

Combustion in catalytic microreactors has applications in portable power generation and process intensification. In this work, catalytic microcombustion of propane in two geometries – *U-bend* and *Spiral*, which have heat recirculation in counter-current and co-current configurations respectively – is investigated computationally. 2D CFD simulations are performed to analyze the performance characteristics of both the reactors and a comparative study is presented. Heat recirculation due to transverse heat transfer occurs in both the geometries. U-bend reactor is more stable than spiral over a wider range of operating conditions due to effective counter-current heat exchange. Spiral reactor has higher peak temperatures due to better internal heat recirculation and lower heat loss to the ambient. Excess enthalpy combustion in both the reactors allows combustion at lean conditions, resulting in lower temperatures and fairly uniform temperature profile, useful for coupling thermoelectrics.

Keywords Excess enthalpy · Co-current heat recirculation · Thermal management · Catalytic combustion · Catalytic microreactors

Introduction

As a consequence of advances in microfabrication techniques, a trend for miniaturization of mechanical devices set in in the past decades [1]. Combustion in such miniature channels with characteristic dimension <1 mm, called microcombustion, was identified to be promising for applications in portable power generation and in process intensification for improving energy efficiency [2, 3]. Heat of combustion can be converted to electricity by coupling with thermoelectrics [4] or thermophotovoltaics [5] for use in portable applications, or utilized for driving endothermic reaction by close thermal coupling with combustion [6].

Highlights
- CFD analysis shows stable lean combustion with uniform heat distribution in U-bend and spiral catalytic reactors
- U-bend microreactor has higher stability due to counter-current heat exchange
- Spiral microreactor has higher peak temperatures due to higher internal heat transfer area

✉ Niket S. Kaisare
nkaisare@iitm.ac.in

[1] Department of Chemical Engineering, Indian Institute of Technology Madras, Chennai 600036, India

Homogeneous combustion has low stability in microchannels as the flames tend to undergo thermal and radical quenching in confined spaces [7, 8]. In this work, the term "stability" is used to refer to the ignited state of the reactor. Although catalytic combustion suffers from enhanced heat loss in microchannels, it also gains from the fast mass transfer rates and is hence found to be more stable in microchannels than homogeneous combustion [2]. Moreover, catalytic combustion requires lower light-off and operating temperatures and is hence useful for microcombustion [9]. Homo-catalytic combustion in microreactors have been investigated, both experimentally and numerically by Mantzaras and co-workers [9–14]. Even when homogeneous reaction lights-off due to high temperatures in catalytic microreactors, its overall contribution reduces as the channel diameter is decreased [13, 15].

Even for catalytic combustion, minimizing heat loss from the reactor is essential for maintaining stability. Recirculation of reaction heat to preheat the cold feed is known to expand the stable operating window of combustors [16]. This concept of internal heat recirculation was first introduced by Lloyd and Weinberg [17] for conventional-sized combustors, as a means to burn low grade fuels in a counter-current heat recirculating geometry called Swiss-roll. The Swiss-roll geometry has been widely studied [18–22] and is popular for causing excess-enthalpy combustion because of large internal surface area

for heat exchange. Reverse flow reactor is also a heat recirculating configuration [7, 23]. Different types of heat recirculation reactors have been widely studied [16, 24–27]. In contrast to these geometries, straight channel reactor shows lower stability because axial heat conduction in the upstream direction is the only mode of heat recirculation [16, 28]. Ronney and coworkers have done substantial work on analyzing heat-recirculating combustors [16, 21, 22, 29–31]. Maruta and co-workers have done seminal work on small-scale combustors [18, 32, 33]. Moreover, effects of geometry and catalyst placement on combustion have been extensively studied by Di Benedetto, Di Sarli and co-workers [34–40].

Regatte and Kaisare [41] have investigated the effect of using structured inserts to improve the stability and performance of straight channel reactor. We had earlier demonstrated spiral geometry as a transverse heat recirculating reactor that support excess enthalpy combustion with better stability compared to a straight channel reactor [42, 43]. This spiral geometry is different than the Swiss-roll (a double-spiral geometry), since the former facilitates transverse heat transfer between adjacent channels with flow in *co-current* direction.

The desired temperature profiles and operating conditions in microcombustion varies for different applications [2]. Power generation from thermoelectric requires relatively lower temperature and uniform temperature profiles were found to yield higher device efficiency [4, 44, 45], whereas higher skin temperatures and uniform temperature distributions were desirable for thermophotovoltaic cells [46, 47]. Thermal integration with endothermic reaction in adjacent channels have been widely investigated with different flow configurations, namely counter-current [48], co-current [49, 50], and cross-flow [51]. Since ensuring stable combustion remains a key challenge, heat recirculation and other approaches to improve stability have been identified as key research directions [2].

We use computational fluid dynamics (CFD) simulations to compare and contrast two heat recirculating geometries – U-bend and spiral microreactors – for catalytic combustion of lean propane/air mixtures. In the U-bend reactor (Fig. 1a), the reaction mixture takes a U-turn at the end opposite to the inlet, flows in counter-current direction and exits from the outlet situated close to the inlet. Spiral reactor (Fig. 1b) has inlet at the center followed by three turns along which the fluid flows and transfers excess enthalpy in co-current direction, and exits from the outlet situated along the periphery. Excess enthalpy combustors with counter-current flow are extensively studied and documented on different geometries. In contrast, the spiral geometry is a unique configuration that facilitates heat recirculation between adjacent channels with co-current flow. We present a comparative study of the two geometries that have different modes (i.e., counter-current and co-current) of transverse heat exchange and analyze the effect of heat recirculation on the behavior of catalytic combustion in microchannels.

Results and discussions

Heat recirculation characteristics

In our previous work [42], an analysis of spiral microreactor was presented. In this section, we analyze the heat recirculation characteristics in the spiral geometry and provide a comparative analysis with the U-bend microreactor, which is known to exhibit heat recirculation between fluids flowing in counter-current directions.

U-bend reactor

The contours of temperature and propane mass fraction in the U-bend reactor, which has flow in the counter-current direction, are shown in Fig. 2a, b, respectively. The feed which is at ambient conditions gets preheated in the inlet channel due to heat recirculation from the reaction zone. For the base case in U-bend reactor considered here, the reaction zone is situated close to the inlet, as seen from Fig. 2c. The dotted and solid lines represent reaction rates on wall-1 and wall-2, respectively. Following the reaction, the product mixture that flows down the channel gets cooled due to heat loss from the outer wall. Later, close to the outlet, this product stream picks up the

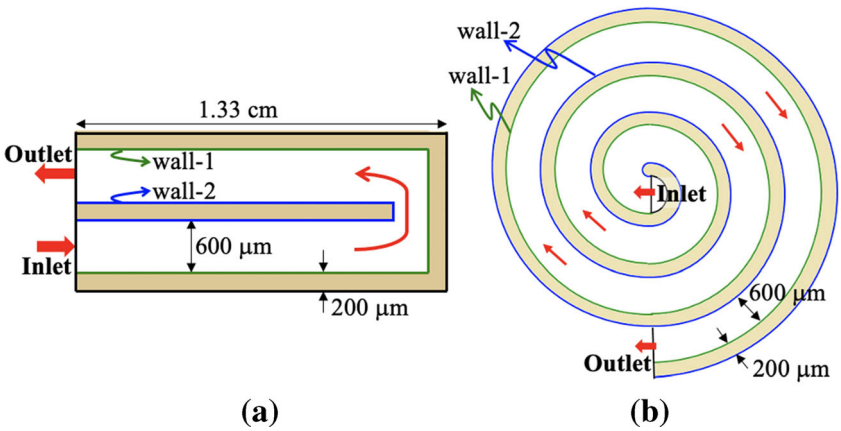

Fig. 1 Schematic of **a** U-bend and **b** spiral microreactors. The schematics are not drawn to scale. Solid block arrows indicate inlet and outlet streams and thin arrows indicate the flow direction. Wall-1 (green line) and wall-2 (blue line) denote the catalytic walls

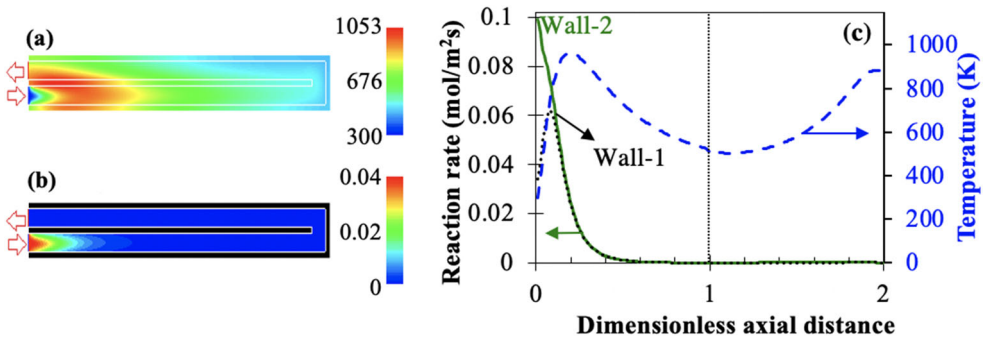

Fig. 2 Contours of **a** temperature in Kelvins and **b** propane mass fraction; and **c** axial profiles of reaction rates on wall-1 (dotted line) and wall-2 (solid line) and temperature along the centerline (dashed blue line, secondary Y-axis) in the U-bend microreactor for the base case. Vertical dashed line indicates separation of inlet and outlet channels in Panel-c

heat released in the reaction zone of the inlet channel and preheats the cold feed. Although the reactor model has walls of low thermal conductivity, axial heat conduction along the inner-wall also contributes to feed preheating. However, this heat transfer is facilitated by the presence of the outlet channel that also acts as a protection for the reaction zone.

The profiles of reaction rates along the catalytic walls and temperature along the centerline of the U-bend reactor are shown in Fig. 2c, with the temperature (dashed lines) plotted on the secondary ordinate. The first half (until $z/L = 1$) represents the inlet channel and the latter half ($1 \le z/L \le 2$) represents the outlet or recirculation channel. Wall-2 is the inner-wall, which separates the reactant and product channels, along which transverse heat transfer occurs. Since wall-2 is comparatively better protected from heat loss due to the adjacent flow channels, it has higher reaction rate than wall-1. The higher temperature of the inner solid wall compared to wall-1 is clearly visible from the contours of Fig. 2a. Since the reaction zone is situated in the first quarter of the reactor, propane mass fraction contour in Fig. 2b reach nearly complete conversion in the initial section of the inlet channel itself. The fully converted mixture in the outlet channel acts as a heat carrier near the outlet of the reactor and preheats the cold inlet. Unlike the downstream region of the reactor, the direction of heat transfer in the initial section is from the outlet channel to the inlet channel indicating heat recirculation.

Spiral reactor

Temperature and mass fraction contours in the spiral microreactor for the base case are shown in Fig. 3. As opposed to the case of U-bend reactor, high temperature zone is spread over a larger part of the reactor, i.e., the reaction zone enters the second turn of the spiral microreactor, as against ~1/3rd of the inlet channel in the U-bend microreactor. The cold feed at the inlet in the first turn gets preheated by the hot products in the second turn of the spiral microreactor. It is interesting to observe that the peak temperature in spiral reactor is more than that in U-bend reactor. This is because outer wall has comparatively lower area and hence the heat lost to the surroundings is lower.

Profiles of reaction rate along both the catalytic walls and temperature along the centerline are plotted in Fig. 4. The maximum reaction rate is lower in the spiral. Unlike the U-bend reactor, the reaction zone is spread out over one turn that is, almost half of the spiral reactor. Reaction rate on wall-1 is higher than that on wall-2. Note that both walls in the first turn of the spiral microreactor are protected from heat loss due to the peripheral channels. However, since wall-1 adjoins the second turn of the reactor, it remains at a temperature higher than that in wall-2 in first turn of the spiral. Figure 4 also shows the temperature profiles (right Y-axis). A consistently higher temperature in the second turn of the spiral indicates that there is transverse heat transfer to the first turn. This transverse heat transfer from the second turn is the primary mode of

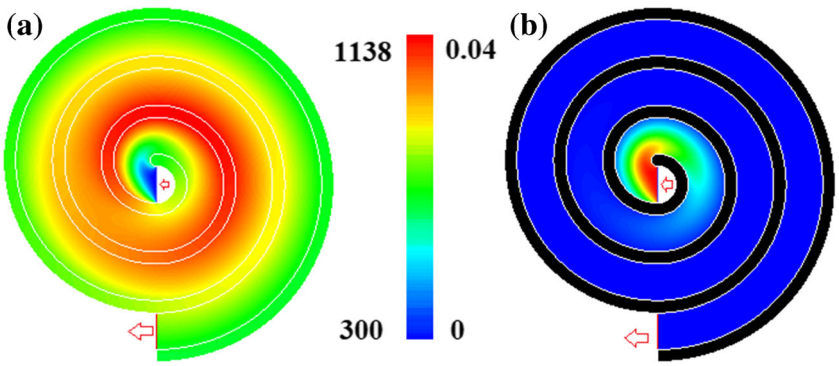

Fig. 3 Contours of **a** temperature (in K) and **b** propane mass fraction in the spiral microreactor for the base case

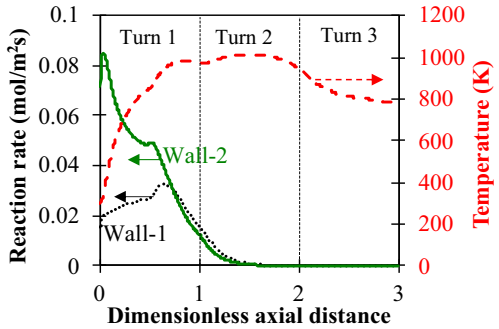

Fig. 4 Profiles of reaction rates on wall-1 (dotted black line) and wall-2 (solid green line), and the temperature along centerline (dashed red line, secondary Y axis) vs. dimensionless axial distance (z/L) in the spiral microreactor. Vertical dashed lines delineate the 3 turns

preheating of the inlet feed in this setup. Moreover, the compact geometry with heat loss only from the outermost turn causes protection of the reaction zone in the inner turns and a uniform heat distribution in the reactor.

In summary, in the spiral microreactor, heat is transferred in transverse direction from the hot fluid in the second turn to the cold inlet feed, flowing in the same direction. Although the maximum reaction rate is lower and the reaction zone is more spread out, the spiral microreactor show a higher maximum temperature. Consequently, a comparison between the two geometries at various operating conditions is presented in the next section.

Comparative study: effect of feed composition and inlet velocity

Figure 5 shows the effect of inlet velocity on the peak temperature and propane conversion in U-bend and spiral microreactors at two different equivalence ratios. Peak temperature increases with increase in inlet velocity because of the higher power input. It is interesting to note that the peak temperature in spiral reactor is higher than that in U-bend reactor for all the cases considered. This result is interesting because the flow in counter-current direction in the U-bend is expected to have a greater recirculation of excess enthalpy [25], compared to the spiral where this heat transfer takes place in co-current direction. However, the maximum temperature in the spiral reactor is higher, which may be due to the fact that it loses lesser heat owing to the lower heat loss area of the outer wall. However, as expected, the counter-current heat transfer in U-bend results in higher region of stable operation than the spiral microreactor. The vertical arrows in Fig. 5 represent the conditions at which the respective system loses stability due to extinction and blowout.

Extinction and blowout are the major causes of instability and the reactor operation is possible only within the stable limits dictated by them. Extinction occurs at lower velocities and equivalence ratios, when the power input is not enough to

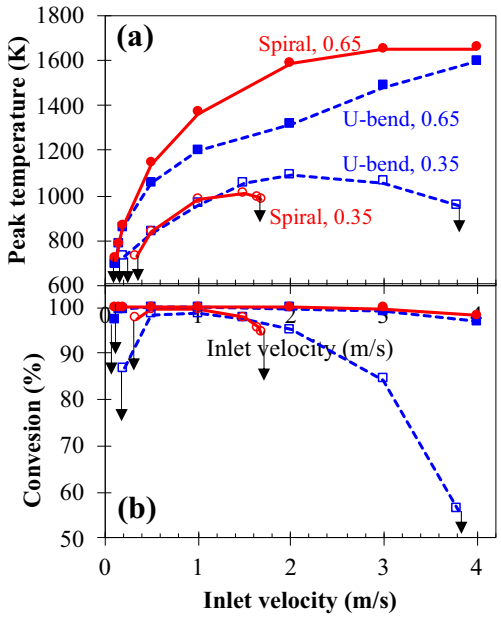

Fig. 5 **a** Peak temperature and **b** propane conversion as a function of inlet velocity for spiral (solid red lines with circle symbols) and U-bend reactors (dashed blue lines with square symbols) for the equivalence ratios of $\phi = 0.65$ (filled symbols) and 0.35 (empty symbols). Downward arrows indicate points of extinction and blowout

sustain combustion and blowout occurs at higher velocities, when the residence time is lesser than the reaction time [28]. In this study, the velocity was varied in the chosen range of 0.1–4 m/s. For $\phi = 0.65$, extinction in spiral reactor occurs at 0.11 m/s and that in U-bend reactor occurs at a slightly lower velocity of 0.1 m/s. There is a slight dip in propane conversion near the extinction point in U-bend reactor. Both reactors sustain combustion up to 4 m/s for $\phi = 0.65$, with conversion exceeding 99% up to 3 m/s. For the more dilute mixture with $\phi = 0.35$, the spiral reactor shows extinction at 0.33 m/s, whereas U-bend shows much higher stability with extinction observed at 0.2 m/s. This is due to the counter-current heat exchange in the U-bend reactor that effectively preheats the feed. In the spiral reactor, at the lower power input at low equivalence ratio, co-current flow along the turns results in heat getting spread out causing extinction. Near the point of extinction, propane conversion is incomplete and the dip in conversion in the U-bend reactor is clearly visible in Fig. 5b. Spiral reactor undergoes blowout at 1.69 m/s for $\phi = 0.35$, beyond which stable combustion is not sustainable. In contrast, U-bend reactor sustains combustion for higher values of inlet velocity, with blowout observed at $u_{in} = 3.81$ m/s. This also indicates that counter-current heat transfer in U-bend reactor is more effective in feed preheating. It should be noted that the straight-channel microreactor, in contrast, did not show stable combustion at the leaner mixture ($\phi = 0.35$).

Figure 6 shows a comparison between temperature in the two geometries at a higher velocity of $u_{in} = 2$ m/s, with all other parameters at their nominal values. The reaction zone

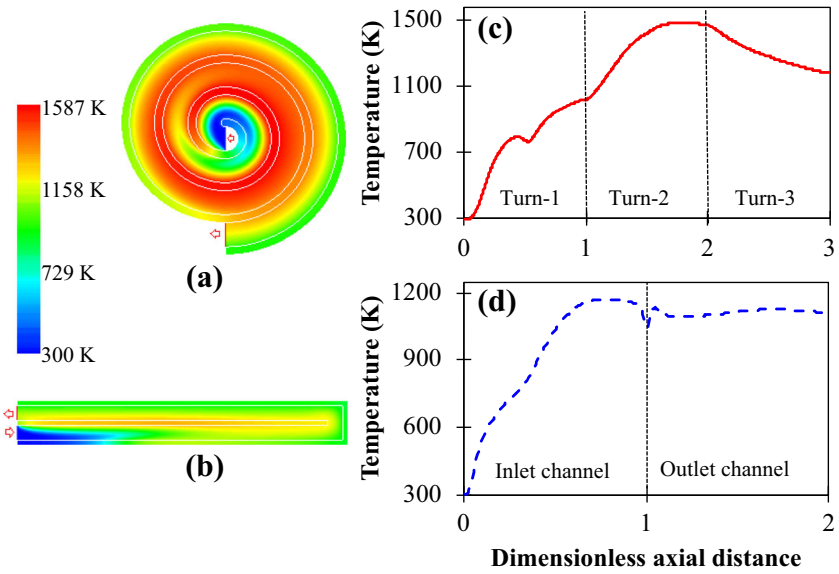

Fig. 6 Temperature contours in **a** spiral microreactor and **b** U-bend microreactor, and (c,d) the corresponding axial profiles of centerline temperatures vs. dimensionless axial distance. These results are shown for a higher inlet velocity $u_{in} = 2$ m/s, and the other parameters kept at their base case values

gets pushed downstream in both geometries and preheating due to heat recirculation occurs in the initial part of the reactor, as evidenced by the delayed appearance of temperature maxima in the axial temperatures shown in Fig. 6c, d. In the spiral reactor, the reaction zone gets pushed to the outer turns, as indicated by the significantly higher temperature in the third turn, in spite of heat losses to the surrounding. This reduces the efficiency of heat transfer since this region is not directly in thermal contact with the cold inlet stream. In contrast, the product stream in the U-bend maintains contact with the cold inlet stream, ensuring more effective heat transfer. There is a significant drop in propane conversion in the U-bend reactor prior to blow out. This implies that in spite of lower residence times (that lead to incomplete conversion), counter-current heat recirculation enables occurrence of some amount of reaction. Thus in terms of effectiveness of heat recirculation, U-bend reactor has an "upper hand" over spiral reactor, where co-current flow along the turns causes protection of the reaction zone than a increased heat recirculation. Cases of higher velocity in U-bend reactor can result in propane breakthrough, although in small quantities. The contours in Fig. 6 indicate that higher inlet velocity results in a more uniform heat distribution in the U-bend reactor.

Peak reactor temperature and propane conversion as a function of equivalence ratios between 0.3 to 0.85 are plotted in Fig. 7 for inlet velocities $u_{in} = 0.5$ and 2 m/s. As already observed, spiral reactor has higher peak temperature than U-bend reactor. At the lower velocities or lower equivalence ratios, the difference in peak temperatures is rather modest. However, the difference in the peak temperature between the two geometries is significant at higher equivalence ratios and higher velocities, where the power input is higher. It is interesting to note that although the peak temperature in spiral microreactor is higher, it is unable to sustain stable combustion at lower equivalence ratios when $u_{in} = 2$ m/s because of blowout instability. On the other hand, U-bend reactor sustains combustion even for $\phi = 0.3$ but with a lower value of propane conversion.

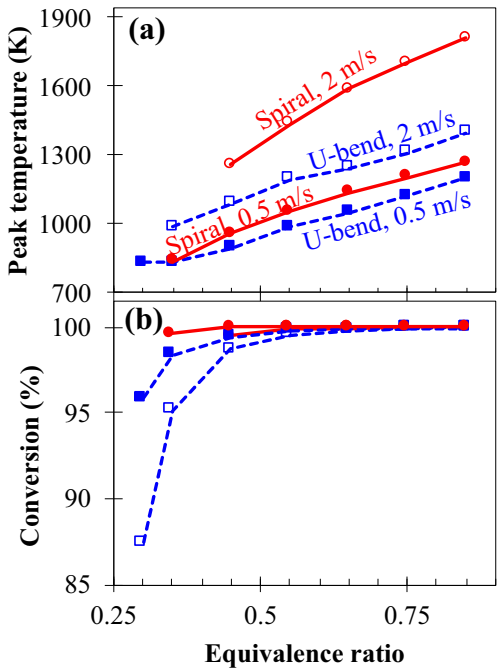

Fig. 7 **a** Peak temperature and **b** propane conversion as a function equivalence ratio for spiral (red, solid lines with circle symbols) and U-bend reactors (blue, dashed lines with square symbols) for the inlet velocity = 0.5 m/s (solid symbols) and 2 m/s (empty symbols)

Both the U-bend and spiral reactors with their characteristic counter and co-current modes of heat recirculation are useful for propane microcombustion. Various applications of such microdevices, such as coupling with thermoelectric or thermophotovoltaics for portable power generation, require fulfillment of certain criteria: better stability, complete propane conversion and desired operating temperatures that depend on the particular application. It is possible to choose the operating conditions that meet such needs. For example, thermoelectric requires more uniform temperature distribution and lower skin temperatures [4]. Figure 8 shows the temperature contours in both the reactors with $\phi = 0.35$ and $u_{in} = 0.5$ m/s. Due to the lower value of equivalence ratio, power input to the system is low, resulting in lower temperatures. The temperature distribution is fairly uniform in both the reactors for this case. Propane conversion exceeds 99.5% for spiral, whereas it is 98.4% for U-bend microreactor. This case is an instance of a feasible operating point for coupling a thermoelectric module. It is interesting to note that at these conditions ($\phi = 0.35$, $u_{in} = 0.5$ m/s), the peak temperature in spiral and U-bend are 838 K and 832 K, respectively.

As can be seen from the contours Fig. 8, the reaction zone gets pushed significantly downstream in both geometries at $\phi = 0.35$, $u_{in} = 0.5$ m/s. The propane contours are skipped for brevity. There is not much reaction in the first half of inlet channel (U-bend) or first turn (spiral). Clearly, when the reaction zone is pushed downstream, a longer length of both the microreactors is utilized for preheating propane-air mixture to its light-off temperature owing to heat recirculation from the adjacent channel in either geometry. In absence of such heat transfer, non-heat-recirculating geometries (such as straight channel) are unable to sustain stable combustion under such lean conditions for propane-air mixtures.

In summary, a comparison with the heat recirculating U-bend geometry provides a clearer evidence so far of the heat

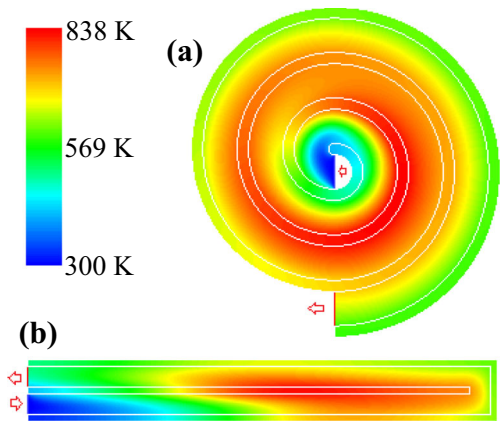

Fig. 8 Temperature contours in **a** spiral microreactor and **b** U-bend microreactor for a lower equivalence ratio $\phi = 0.35$. Other parameters are same as that in the base case

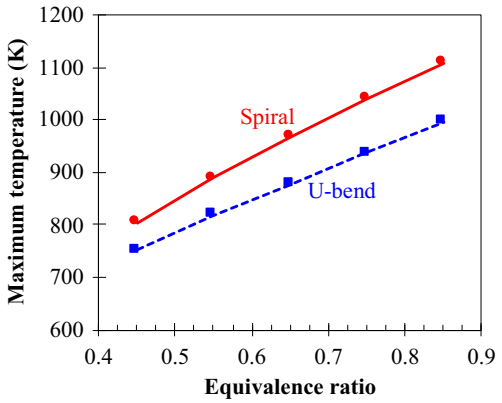

Fig. 9 Maximum temperature as a function of equivalence ratio for spiral (red, solid lines with circle symbols) and U-bend reactors (blue, dashed lines with square symbols) when steel walls are considered ($k_s = 16.27$ W/m.K) All other parameters are same as that in the base case

recirculation in the spiral microreactor. The increased efficiency of transverse heat transfer when the reaction zone was pushed downstream resulted in increased temperature at higher velocity. On the other hand, when the reaction zone was pushed to the outer turn, spiral showed similar peak temperature as the U-bend microreactor. The results indicate that for practical applications of microcombustion, it is possible to tune the operating conditions in both geometries to ensure appropriate temperature, propane conversion and device stability. Though the straight-channel geometry may arguably be easier to fabricate, the heat recirculating geometries are advantageous in all other aspects.

Effect of thermal conductivity

Increasing the thermal conductivity of the walls is known to result in a better uniformity of heat distribution due to heat

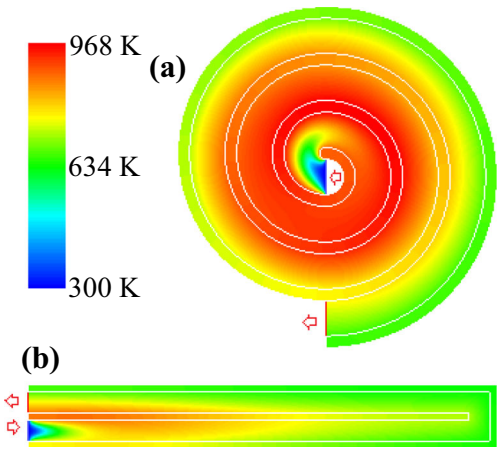

Fig. 10 Temperature contours in **a** spiral microreactor and **b** U-bend microreactor for a higher wall conductivity of 16.27 W/m.K, representing moderately conducting materials such as steel. Other parameters are same as that in the base case

Table 1 Various parameters and their nominal values. The geometry and sizes of the spiral microreactor are same as those in our previous work [22], whereas those of the U-bend microreactor are chosen to match the spiral geometry

Parameters		Values
Channel gap size	d	600 μm
Reactor wall thickness	b_w	200 μm
Axial length of reactor*	L	2.64 cm
Wall thermal conductivity	k_s	1, 16.3 W/m.K
Equivalence ratio	ϕ	0.3–0.85 (0.65)
Convective coefficient	h_∞	10 W/m^2.K
Emissivity	ε	0.9
Inlet velocity	u_{in}	0.1–4 (0.5 m/s)

*Measured along the centerline

conduction, thus lowering the peak temperatures. At the same time, higher wall thermal conductivity also makes the reactor more susceptible to extinction instability. Figure 9 depicts the peak temperature as a function of equivalence ratio, attained in the spiral and U-bend microreactors with steel walls (k_s = 16.27 W/mK) and base case velocity of u_{in} = 0.5 m/s. As expected, the peak temperatures in spiral are lower than those observed for k_s = 1 W/m.K in the previous section. The spiral reactor continues to have higher peak temperature than U-bend reactor due to the difference in heat loss area of outer-walls. In fact, the difference between the peak temperatures of both the reactors is more in the case of steel reactor, compared to the equivalent cases in a ceramic reactor. Propane conversion is 100% for all the cases plotted.

Figure 10 depicts the temperature contours in both the reactors for the base case equivalent in steel reactor. Compared to Figs. 2a and 3a, the temperatures are more uniform when solid material with higher conductivity is used. The spiral reactor displays uniform temperature distribution, with most of the reaction occurring in the first two turns, whereas the external wall is at a lower temperature owing to heat loss. The U-bend reactor also shows a fairly uniform temperature distribution. Use of materials with high thermal conductivity for reactor fabrication may be adopted to attain uniform temperature profiles, which would be advantageous for coupling with applicative devices like thermoelectric, where uniform temperatures are preferred for higher power generation.

Table 2 Kinetic parameters for lean propane/air combustion on Pt catalyst

	A (s^{-1}) or s_i	β	E (kcal/mol)
C_3H_8 adsorption	0.06	0.154	4
O_2 adsorption	0.0542	0.766	0
O_2 desorption	8.41×10^{12}	−0.796	Eq. (16)

Conclusions

The U-bend and spiral microreactors are both heat recirculating geometries that support excess enthalpy combustion. It is well-known that the former shows heat recirculation between hot product and cold inlet streams flowing in counter-current directions, whereas the spiral microreactor shows heat recirculation between adjacent turns with fluids flowing in co-current direction. The more efficient counter-current heat transfer in the U-bend reactor setup resulted in stable combustion, of lean propane/air on Pt catalyst, over a wide range of operating conditions. In contrast, the spiral reactor possesses higher ratio of internal heat exchange area to the external heat loss area, resulting in higher peak temperatures than the U-bend for all conditions investigated in this work. In other words, higher peak temperatures can be attributed to both heat recirculation to the cold inlet feed in the first turn as well as the lower area of heat loss in the spiral microreactor. Due to the compact nature of the spiral geometry, heat distribution remains fairly uniform for most operating conditions. Using materials with higher thermal conductivity can help attain more uniform temperature distribution. We showed the possibility of choosing operating conditions to meet requirements of various microcombustion applications. For example, uniform temperature, high propane conversion, and low peak temperature could be attained in both geometries at very lean conditions of ϕ = 0.35, which are conducive for coupling with thermoelectric devices for power generation.

The two geometries were compared for a wide range of inlet velocity and equivalence ratio for lean propane-air mixtures. At higher velocities, where the reaction gets pushed significantly downstream in the micro-channel, more surface area was available for reactant preheating, resulting in higher peak temperatures in spiral geometry. However, when the reaction zone reaches the outer turn of the spiral reactor, loss of stability due to blowout was observed. In contrast, more efficient heat recirculation in the counter current direction in the U-bend resulted in a wider region of stable combustion, albeit with propane breakthrough due to incomplete conversion. Based on the advantages of spiral and U-bend geometry, a serpentine reactor with counter-current flow, where fluid takes two turns may be designed to take advantage of both counter-current heat transfer and large internal heat transfer area. Such a reactor may provide higher temperatures with better stability, and needs to be investigated and compared to spiral reactor in future.

Methodology

Reactor geometry

Schematics of the U-bend and spiral reactors in 2D were shown in Fig. 1. The U-bend reactor could be thought of a

single channel that is bent at 180° one end, with the inlet and outlet situated on the same side and the reaction mixture taking a U-turn on the opposite end, resulting in counter-current flow of the streams across the dividing wall (Fig. 1a). Spiral reactor has inlet at the center and outlet along the periphery, with the reaction mixture spiraling outward from the center (Fig. 1b). The adjacent channels in the spiral microreactor have fluids flowing along the same direction (co-current). In 3D, the flow in inlet channel of the spiral reactor would be in the direction perpendicular to this flow direction. In this work, the reactors are modelled in 2D considering the depth (in the third dimension) to be significantly larger. In both geometries, changing from 3D to 2D geometry is unlikely to make a difference in their qualitative behavior as the flow direction is as modeled in the 2D. However, in the case of spiral reactor in 3D, preheating would occur in the inlet channel also. Yet, 2D is a reasonable approximation for comparison [43]. All the inner-walls (denoted as wall-1 and wall-2) are catalytic, and reaction is enabled on them. The axial length along centerline of the 3-turn spiral reactor is 2.64 cm and for fair comparison, the U-bend reactor having an equivalent length along the centerline is considered for the study. The reactor dimensions as well as operating parameters are summarized in Table 1.

Model description and computational methodology

Two-dimensional CFD simulations are setup in ANSYS Fluent for laminar flow with reactions enabled. The second order upwind differencing is used for spatial discretization of all equations and SIMPLE algorithm is used for pressure-velocity coupling. The mass, momentum, species and energy balance equations are solved for the fluid phase, and the energy balance equation for the solid phase.

The assumptions considered in the model are: (i) steady state; (ii) laminar flow (due to low Re); (iii) ideal gas; (iv) no radiation on the inner-walls; (v) no effect of gravity; (vi) no homogeneous reactions; and (vii) catalytic reactions occur on the inner-walls (wall-1 and wall-2). The equations solved are the continuity, momentum, energy and balances of the reactive species, namely C_3H_8, O_2, CO_2, H_2O. The following are the governing equations:

Continuity equation:

$$\nabla.(\rho \boldsymbol{v}) = 0 \tag{1}$$

Momentum balance equations:

$$\nabla.(\rho \boldsymbol{v}\boldsymbol{v}) + \nabla p - \nabla.\left[\mu\left(\nabla \boldsymbol{v} + \nabla \boldsymbol{v}^T\right) - \frac{2}{3}(\mu \nabla.\boldsymbol{v})\boldsymbol{I}\right] = 0 \tag{2}$$

Species balance (for $k \leq n_{sg}$):

$$\nabla.(\rho \boldsymbol{v} Y_k) + \nabla.(\rho Y_k \mathbf{V}_k) = 0 \tag{3}$$

where, the species diffusion velocity is calculated, accounting for thermal diffusion, as:

$$\mathbf{V}_k = -\frac{D_{km}}{Y_k}\nabla Y_k - \frac{D_k^T}{\rho Y_k}\frac{\nabla \mathrm{T}}{T} \tag{4}$$

Energy balance in the gas:

$$\nabla.(\rho h \boldsymbol{v}) + \nabla.\left(\rho \sum_{k=1}^{n_{sg}} Y_k h_k \mathbf{V}_k\right) - \nabla.\left(\lambda_g \nabla T\right) = 0 \tag{5}$$

Energy balance in the solid:

$$\lambda_s \nabla^2 T = 0 \tag{6}$$

The solver is pressure-based, with absolute velocity formulation. The mixture is modelled as an ideal gas and specific heat, thermal conductivity and viscosity are computed using mixing law. The physical properties of each gas-phase species are temperature-dependent. The density is calculated using ideal gas law, the specific heats are calculated using a piece-wise polynomial function of temperature, and the transport properties of the gases (viz., diffusivity, viscosity and thermal conductivity) are calculated using kinetic theory. These parameters were taken from ANSYS Fluent database [52], and are also available from NIST [53] or other databases.

The physical properties of the solid walls are assumed constant and invariant with temperature. The wall thermal conductivity for the base case is 1 W/m.K to represent ceramic material. Simulations with steel (k_s = 16.3 W/m.K), which has an order of magnitude higher thermal conductivity, are also presented.

Dirichlet boundary conditions for mass, momentum and energy were used at the reactor inlets, as given in the Table 1.

$$\begin{aligned} &\text{At inlet}: v_x = v_{x,\mathrm{in}},\quad Y_k = Y_{k,\mathrm{in}},\quad T = T_{\mathrm{in}}, \\ &\text{At outlet}: p = p_{out} \end{aligned} \tag{7}$$

The inlet temperature is T_{in} = 300 K and pressure p_{out} = 1 atm for all the cases. The inlet velocity and equivalence ratio are varied, with u_{in} = 0.5 m/s and ϕ = 0.65 chosen for the base case, respectively.

The outer walls of both the reactors lose heat by convection (h_{loss} = 10 W/m^2.K) and radiation (ε = 0.9) to the ambient, which is at 300 K:

$$\text{At outer walls}: q_{loss} = h_{\mathrm{loss}}\left(T_{\mathrm{oWall}} - T_\infty\right) + \varepsilon\sigma\left(T_{\mathrm{owall}}^4 - T_\infty\right) \tag{8}$$

At all the inner walls (i.e., at all the solid-gas inter-faces), the no-slip boundary condition is used, and the reaction is enabled:

$$\boldsymbol{v} = 0 \text{ (No-slip condition)} \tag{9}$$

$$\left(\rho Y_k \boldsymbol{V_{k,y}}\right)_{R_{\text{wall}}} + W_k(R_k)_{\text{R}_{\text{wall}}} = 0, \quad R_k = \sum_{i=1}^{n_{rxn}} \nu_{ik} r_i \eta \tag{10}$$

$$-\lambda_g \left(\frac{\partial T}{\partial y}\right)_{R_{\text{wall}}-} + \lambda_s \left(\frac{\partial T}{\partial y}\right)_{R_{\text{wall}}+} + \sum_{k=1}^{n_{sg}} (R_k h_k W_k) = 0 \tag{11}$$

The core-wall of the spiral reactor (the one that abuts the inlet) loses heat to the incoming fluid by convection at a constant h = 200 W/m^2.K.

The following propane combustion reaction

$$C_3H_8(g) + 5O_2(g) \rightarrow 3CO_2(g) + 4H_2O(g) \tag{12}$$

occurring on the catalyst surface, is included using Fluent user-defined function (UDF). The reaction kinetics on Pt catalyst is given by a single-step reduced-order mechanism derived by Deshmukh and Vlachos [32] via a posteriori reduction of detailed microkinetic model:

$$r = \frac{k^{ads}_{C_3H_8} C_{s,C_3H_8}}{\left(1 + \sqrt{k^{ads}_{O2} C_{s,O2} / k^{des}_{O2}}\right)^2} \tag{13}$$

$$k_i^{ads} = \frac{s_i}{\Gamma} \sqrt{\frac{RT}{2\pi \text{M}_\text{i}}}\, T_r^{\beta_i} e^{-E_i^{ads}/RT} \tag{14}$$

$$k_i^{des} = A_i T_r^{\beta_i^{des}} e^{-E_i^{des}/RT} \tag{15}$$

where, $\Gamma = 2.9 \times 10^9$ mol/cm^2 is the site density, $\eta = 1.7$ is the catalyst surface area factor, $T_r = T/300$ is the dimensionless temperature. The rate parameters for Eq. (2–4) are provided in Table 2 and a detailed explanation of the parameters and the equations can be found in [41]. Under fuel lean burn conditions and atmospheric pressure, the simplified equation for desorption of Oxygen(E^{des}_{O2} in kcal/mol.K) is:

$$E^{\text{des}}_{\text{O}_2} = 0.126T_r^4 - 1.849T_r^3 + 9.124T_r^2 - 13.253T_r + 23.903 \tag{16}$$

A user defined function (UDF) is used in the Fluent solver to compute the rate of the catalytic reaction. Due to the low gap size in this study, homogenous combustion is ignored [42], and $r_{gas} = 0$. This mechanism was validated previously using fixed-bed [54] and microreactor [28] experiments.

The steady state models are solved with the reactors initialized at ignited state for all the simulations. Homogeneous chemistry was neglected because of short gap size of reactor, lower inlet temperature and velocities and higher heat loss considered in this work [15]. Although occurrence of high temperatures could cause homogeneous combustion, the comparative results presented in this work would still hold good because catalytic combustion determines the stability limits. The computational domains of both the reactors are ensured grid independent. The grid independent mesh for U-bend reactor consists of 11,970 elements with 133 divisions in the axial direction, and 30 and 10 divisions in the transverse direction in the fluid and solid zones respectively. For the spiral reactor, a non-uniform, biased mesh is used in the transverse direction in the fluid zone. A spacing of approx. 7.6E-6 m at the wall reaction zone and 6.2E-5 m at the center of the channel is used. The solid wall zone in the transverse direction has 8 uniform divisions. In the axial direction, each turn is divided into 200 elements, totaling to 600 axial elements for the 3-turn reactor. Axial grid spacing successively reduces with decreasing radial distance towards the spiral center to account for the change in the curvature in case of the reactor. An interested reader is referred to our previous work for more details on the computational methodology and grid independence [22].

Acknowledgements The authors thank Mr. Amit Kunte for helping with the model development and initial simulations.

Declarations

Conflict of interest On behalf of all authors, the corresponding author states that there is no conflict of interest.

References

1. Fernandez-Pello AC (2002) Micropower generation using combustion: issues and approaches. Proc Combust Inst 29:883–899. https://doi.org/10.1016/S1540-7489(02)80113-4
2. Kaisare NS, Vlachos DG (2012) A review on microcombustion: fundamentals, devices and applications. Prog Energy Combust Sci 38:321–359. https://doi.org/10.1016/j.pecs.2012.01.001
3. Ju Y, Maruta K (2011) Microscale combustion: technology development and fundamental research. Prog Energy Combust Sci 37:669–715. https://doi.org/10.1016/j.pecs.2011.03.001
4. Federici JA, Norton DG, Bruggemann T, Voit KW, Wetzel ED, Vlachos DG (2006) Catalytic microcombustors with integrated thermoelectric elements for portable power production. J Power Sources 161:1469–1478. https://doi.org/10.1016/j.jpowsour.2006.06.042
5. Yang WM, Chou SK, Shu C, Xue H, Li ZW, Li DT, Pan JF (2003) Microscale combustion research for application to micro thermophotovoltaic systems. Energy Convers Manag 44:2625–2634. https://doi.org/10.1016/S0196-8904(03)00024-4
6. Kolios G, Frauhammer J, Eigenberger G (2000) Autothermal fixed-bed reactor concepts. Chem Eng Sci 55:5945–5967. https://doi.org/10.1016/S0009-2509(00)00183-4
7. Kaisare NS, Vlachos DG (2007) Extending the region of stable homogeneous micro-combustion through forced unsteady operation. Proc Combust Inst 31 II:3293–3300. https://doi.org/10.1016/j.proci.2006.07.031
8. Aghalayam P, Bui P-A, Vlachos DG (1998) The role of radical wall quenching in flame stability and wall heat flux: hydrogen-air mixtures. Combust Theory Model 2:515–530. https://doi.org/10.1088/1364-7830/2/4/010
9. Karagiannidis S, Mantzaras J, Jackson G, Boulouchos K (2007) Hetero−/homogeneous combustion and stability maps in methane-

fueled catalytic microreactors. Proc Combust Inst 31 II:3309–3317. https://doi.org/10.1016/j.proci.2006.07.121
10. Appel C, Mantzaras J, Schaeren R, Bombach R, Inauen A, Kaeppeli B, Hemmerling B, Stampanoni A (2002) An experimental and numerical investigation of homogeneous ignition in catalytically stabilized combustion of hydrogen/air mixtures over platinum. Combust Flame 128:340–368. https://doi.org/10.1016/S0010-2180(01)00363-7
11. Mantzaras J, Appel C (2002) Effects of finite rate heterogeneous kinetics on homogeneous ignition in catalytically stabilized channel flow combustion. Combust Flame 130:336–351. https://doi.org/10.1016/S0010-2180(02)00384-X
12. Mantzaras J, Bombach R, Schaeren R (2009) Hetero−/homogeneous combustion of hydrogen/air mixtures over platinum at pressures up to 10 bar. Proc Combust Inst 32 II:1937–1945 . https://doi.org/10.1016/j.proci.2008.06.067
13. Karagiannidis S, Marketos K, Mantzaras J, Schaeren R, Boulouchos K (2010) Experimental and numerical investigation of a propane-fueled, catalytic mesoscale combustor. Catal Today 155:108–115. https://doi.org/10.1016/j.cattod.2010.04.030
14. Dogwiler M, Benz K, Bombach A (1998) Homogeneous ignition of methane-air mixtures over platinum: comparison of measurements and detailed numerical predictions. Symp Combust 2:2275–2282. https://doi.org/10.1016/S0082-0784(98)80077-5
15. Stefanidis GD, Vlachos DG (2009) Controlling homogeneous chemistry in homogeneous-heterogeneous reactors: application to propane combustion. Ind Eng Chem Res 48:5962–5968. https://doi.org/10.1021/ie801480m
16. Ronney PD (2003) Analysis of non-adiabatic heat-recirculating combustors. Combust Flame 135:421–439. https://doi.org/10.1016/j.combustflame.2003.07.003
17. Lloyd SA, Weinberg FJ (1974) A burner for mixtures of very low heat content. Nature 251:47–49. https://doi.org/10.1038/251047a0
18. Kim NI, Aizumi S, Yokomori T, Kato S, Fujimori T, Maruta K (2007) Development and scale effects of small Swiss-roll combustors. Proc Combust Inst 31 II:3243–3250. https://doi.org/10.1016/j.proci.2006.08.077
19. Zhong BJ, Wang JH (2010) Experimental study on premixed CH4/air mixture combustion in micro Swiss-roll combustors. Combust Flame 157:2222–2229. https://doi.org/10.1016/j.combustflame.2010.07.014
20. Ju Y, Choi CW (2003) An analysis of sub-limit flame dynamics using opposite propagating flames in mesoscale channels 133:483–493 . https://doi.org/10.1016/S0010-2180(03)00058-0
21. Kuo CH, Ronney PD (2007) Numerical modeling of non-adiabatic heat-recirculating combustors. Proc Combust Inst 31 II:3277–3284. https://doi.org/10.1016/j.proci.2006.08.082
22. Chen C-H, Ronney PD (2011) Effects of scale on Swiss-roll heat recirculaing combustors. 23rd International Colloquium on the Dynamics of Explosions and Reactive Systems (ICDERS), Irvine, CA, Paper-0306
23. Eigenberger G, Nieken U (1988) Catalytic combustion with periodic flow reversal. Chem Eng Sci 43:2109–2115. https://doi.org/10.1016/0009-2509(88)87091-X
24. Federici JA, Wetzel ED, Geil BR, Vlachos DG (2009) Single channel and heat recirculation catalytic microburners: an experimental and computational fluid dynamics study. Proc Combust Inst 32 II:3011–3018. https://doi.org/10.1016/j.proci.2008.07.005
25. Schoegl I, Ellzey JL (2007) Superadiabatic combustion in conducting tubes and heat exchangers of finite length. Combust Flame 151:142–159. https://doi.org/10.1016/j.combustflame.2007.01.009
26. Chen J, Song W, Gao X, Yan L, Xu D (2016) Flame stability of propane-air premixed combustion in heat-recirculation micro-combustors. Front Heat Mass Transf 7:1–9. https://doi.org/10.5098/hmt.7.3
27. Chen J, Yan L, Song W, Xu D (2017) Effect of heat recirculation on the combustion stability of methane-air mixtures in catalytic micro-combustors. Appl Therm Eng 115:702–714. https://doi.org/10.1016/j.applthermaleng.2017.01.031
28. Kaisare NS, Deshmukh SR, Vlachos DG (2008) Stability and performance of catalytic microreactors: simulations of propane catalytic combustion on Pt. Chem Eng Sci 63:1098–1116. https://doi.org/10.1016/j.ces.2007.11.014
29. Chen C-H, Ronney PD (2013) Scale and geometry effects on heat-recirculating combustors. Combust Theory Model 17:888–905. https://doi.org/10.1080/13647830.2013.812807
30. Chen CH, Ronney PD (2011) Three-dimensional effects in counterflow heat-recirculating combustors. Proc Combust Inst 33:3285–3291. https://doi.org/10.1016/j.proci.2010.06.081
31. Ahn J, Eastwood C, Sitzki L, Ronney PD (2005) Gas-phase and catalytic combustion in heat-recirculating burners. Proc Combust Inst 30 II: 2463–2472. https://doi.org/10.1016/j.proci.2004.08.265
32. Maruta K (2011) Micro and mesoscale combustion. Proc Combust Inst 33:125–150. https://doi.org/10.1016/j.proci.2010.09.005
33. Kim NI, Kato S, Kataoka T, Yokomori T, Maruyama S, Fujimori T, Maruta K (2005) Flame stabilization and emission of small Swiss-roll combustors as heaters. Combust Flame 141:229–240. https://doi.org/10.1016/j.combustflame.2005.01.006
34. Di Benedetto A, Di Sarli V, Russo G (2009) A novel catalytic-homogenous micro-combustor. Catal Today 147:156–161. https://doi.org/10.1016/j.cattod.2009.07.030
35. Di Benedetto A, Di Sarli V, Russo G (2010) Effect of geometry on the thermal behavior of catalytic micro-combustors. Catal Today 155:116–122. https://doi.org/10.1016/j.cattod.2009.01.048
36. Di Sarli V, Trofa M, Di Benedetto A (2020) A novel catalytic micro-combustor inspired by the nasal geometry of reindeer: Cfd modeling and simulation. Catalysts:10. https://doi.org/10.3390/catal10060606
37. Landi G, Di Benedetto A, Barbato PS, Russo G, Di Sarli V (2014) Transient behavior of structured LaMnO3 catalyst during methane combustion at high pressure. Chem Eng Sci 116:350–358. https://doi.org/10.1016/j.ces.2014.04.029
38. Di Sarli V, Barbato PS, Di Benedetto A, Landi G (2015) Start-up behavior of a LaMnO3 partially coated monolithic combustor at high pressure. Catal Today 242:200–210. https://doi.org/10.1016/j.cattod.2014.07.052
39. Barbato PS, Di Benedetto A, Di Sarli V, Landi G, Pirone R (2012) High-pressure methane combustion over a perovskyte catalyst. Ind Eng Chem Res 51:7547–7558. https://doi.org/10.1021/ie201736p
40. Barbato PS, Di Sarli V, Landi G, Di Benedetto A (2015) High pressure methane catalytic combustion over novel partially coated LaMnO3-based monoliths. Chem Eng J 259:381–390. https://doi.org/10.1016/j.cej.2014.07.123
41. Regatte VR, Kaisare NS (2011) Propane combustion in non-adiabatic microreactors: 1. Comparison of channel and posted catalytic inserts. Chem Eng Sci 66:1123–1131. https://doi.org/10.1016/j.ces.2010.12.017
42. Kunte A, Raghu AK, Kaisare NS (2018) A spiral microreactor for improved stability and performance for catalytic combustion of propane. Chem Eng Sci 187:87–97. https://doi.org/10.1016/j.ces.2018.04.069
43. Yedala N, Raghu AK, Kaisare NS (2019) A 3D CFD study of homogeneous-catalytic combustion of hydrogen in a spiral microreactor. Combust Flame 206:441–450. https://doi.org/10.1016/j.combustflame.2019.05.022
44. Karim AM, Federici JA, Vlachos DG (2008) Portable power production from methanol in an integrated thermoeletric/microreactor system. J Power Sources 179:113–120. https://doi.org/10.1016/j.jpowsour.2007.12.119
45. Admasu BT, Luo X, Yao J (2013) Effects of temperature non-uniformity over the heat spreader on the outputs of thermoelectric

power generation system. Energy Convers Manag 76:533–540. https://doi.org/10.1016/j.enconman.2013.08.004
46. Yang WM, Chou SK, Shu C, Li ZW, Xue H (2004) A prototype microthermophotovoltaic power generator. Appl Phys Lett 84: 3864–3866. https://doi.org/10.1063/1.1751614
47. Wenming Y, Siawkiang C, Chang S, Hong X, Zhiwang L (2005) Effect of wall thickness of micro-combustor on the performance of micro-thermophotovoltaic power generators. Sensors Actuators A Phys 119:441–445. https://doi.org/10.1016/j.sna.2004.10.005
48. Deshmukh SR, Vlachos DG (2005) CFD simulations of coupled, countercurrent combustor/reformer microdevices for hydrogen production. Ind Eng Chem Res 44:4982–4992
49. Kaisare NS, Stefanidis GD, Vlachos DG (2009) Millisecond production of hydrogen from alternative, high hydrogen density fuels in a cocurrent multifunctional microreactor. Ind Eng Chem Res 48: 1749–1760. https://doi.org/10.1021/ie800392z
50. Lopez E, Gepert V, Gritsch A, Nieken U, Eigenberger G (2012) Ethanol steam reforming thermally coupled with fuel combustion in a parallel plate reactor. Ind Eng Chem Res 51:4143–4151. https://doi.org/10.1021/ie202364y
51. Regatte VR, Kaisare NS (2013) Hydrogen generation in spatially coupled cross-flow microreactors. Chem Eng J 215–216:876–885. https://doi.org/10.1016/j.cej.2012.11.091
52. ANSYS® Fluent 17.2 Academic, Documentation. ANSYS, Inc.
53. Linstrom PJ, Mallard WG NIST Chemistry WebBook, NIST Standard Reference Database Number 69. National Institute of Standards and Technology, Gaithersburg MD, 20899
54. Deshmukh SR, Vlachos DG (2007) A reduced mechanism for methane and one-step rate expressions for fuel-lean catalytic combustion of small alkanes on noble metals. Combust Flame 149:366–383. https://doi.org/10.1016/j.combustflame.2007.02.006